Polar Front around the Kerguelen Islands: An up-to-date determination and associated circulation of surface/subsurface waters

Young-Hyang Park, Isabelle Durand, Élodie Kestenare, Gilles Rougier, Meng Zhou, Francesco d'Ovidio, Cédric Cotté, Jae-Hak Lee

Polar Front around the Kerguelen Islands: An up-to-date determination and associated circulation of surface/subsurface waters

Young-Hyang Park[1], Isabelle Durand[1], Elodie Kestenare[2], Gilles Rougier[3], Meng Zhou[4], Francesco d'Ovidio[5], Cédric Cotté[1], and Jae-Hak Lee[6]

[1]MNHN-Sorbonne Universités (UPMC, Univ Paris 06)-CNRS-IRD, LOCEAN Laboratory, Muséum National d'Histoire Naturelle, Paris, France, [2]LEGOS (IRD/CNES/CNRS/Université Toulouse III), Observatoire Midi-Pyrénées, Toulouse, France, [3]LOPB, Centre d'Océanologie de Marseille, Marseille, France, [4]University of Massachusetts, Boston, Massachusetts, USA, [5]Sorbonne Universités (UPMC, Univ Paris 06)-CNRS-IRD-MNHN, LOCEAN Laboratory, Paris, France, [6]Korea Institute of Ocean Science and Technology, Ansan, South Korea

Abstract The circulation of iron-rich shelf waters around the Kerguelen Islands plays a crucial role for a climatically important, annually recurrent phytoplankton spring bloom over the sluggish shelf region and its downstream plume area along the Antarctic circumpolar flow. However, there is a long-standing confusion about the Polar Front (PF) in the Kerguelen region due to diverse suggestions in the literature for its geographical location with an extreme difference over 10° of latitude. Based on abundant historical hydrographic data, the in situ hydrographic and current measurements during the 2011 KEOPS2 cruise, satellite chlorophyll images, and altimetry-derived surface velocity fields, we determine and validate an up-to-date location of the PF around the Kerguelen Islands. Artificial Lagrangian particle trajectories computed from altimetric velocity time series are analyzed for the possible pathways and sources of different surface/subsurface waters advected into the chlorophyll bloom area east off the islands studied during the KEOPS2 cruise. The PF location determined as the northernmost boundary of the Winter Water colder than 2°C, which is also associated with a band of strong currents, appears to be primarily controlled by topography. The PF rounds the Kerguelen Islands from the south to deflect northward along the eastern escarpment up to the northeastern corner of the Kerguelen Plateau before making its southward retroflection. It is shown that the major surface/subsurface waters found within the deep basin east of the Kerguelen Islands originate from the shelf around the Heard Island, rather than from the shallow shelf north of the Kerguelen Islands.

1. Introduction

The Kerguelen Plateau forms a major topographic barrier to the deep-reaching Antarctic Circumpolar Current (ACC), except for three deep passages such as the Kerguelen-Amsterdam passage north of the Kerguelen Plateau, the Fawn Trough dividing the Kerguelen Plateau at about 56°S into the northern and southern plateaux, and the Princess Elizabeth Trough between the southern tip of the southern plateau and Antarctica. According to direct observations of transport across the Fawn Trough during the 2009 TRACK (TRansport ACross the Kerguelen plateau) cruise [*Park et al.*, 2009] together with previous geostrophic transport estimates in the Kerguelen-Amsterdam passage [*Park et al.*, 1993], about 60% of the total ACC transport ($\sim$150 Sv; 1 Sv $= 10^6$ m^3 s^{-1}) transiting through the Kerguelen region passes north of the Kerguelen Plateau, mostly associated with the Subantarctic Front (SAF). The rest 40% passes across the vast plateau between the Kerguelen Islands and Antarctica, most of which (43 Sv) is concentrated in the Fawn Trough in association with the Southern ACC front (SACCF). There are two secondary branches of transport over the northern plateau identified [*Park et al.*, 2009]; one carries a transport of 6 Sv, passing south of the Heard Island before curling anticyclonically to flow northwestward along the eastern side of the plateau, and partly peeling off from the plateau into the deep Australian-Antarctic Basin, and the other carries a smaller transport ($\sim$2 Sv), hugging the Kerguelen Islands from the south and attaching tightly to the eastern slope of the plateau where it joins the transport coming from the south. Consequently, at the Polar Front (PF) immediately east of the Kerguelen Islands, a combined transport of the above two confluent branches has been estimated approximately $\sim$6 Sv [*Park et al.*, 2009].
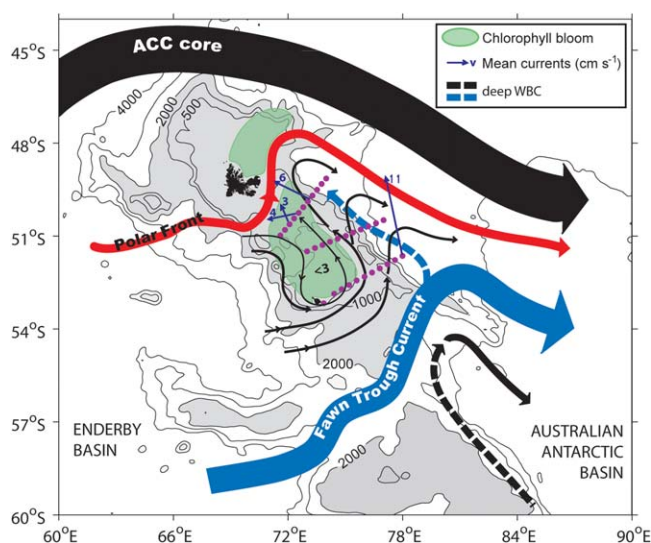
Figure 1. Schematic of the general circulation over and around the Kerguelen Plateau. Adapted from *Park et al.* [2008c].

The northern Kerguelen Plateau especially the central to eastern part of the shelf between the Kerguelen and Heard Islands (where a maximum sill depth is about 650 m) had been the subject of extensive hydrographic and velocity observations during the 2005 KEOPS1 (KErguelen Ocean Plateau compared Study 1) cruise [*Park et al.*, 2008c]. The circulation in this shelf region is relatively stagnant (<5 cm s^{-1}, on average) and anticyclonic (Figure 1), where only the surface/subsurface water masses (Antarctic Surface Water and Winter Water) form the predominant water masses. The annually recurrent enhanced primary production over the plateau is confined within the shallow stagnant area probably because of enhanced vertical transfer of iron due to elevated vertical mixing associated with strong internal tides [*Park et al.*, 2008b], in addition to the horizontal advection of iron-rich water originated from the Heard Island [*van Beek et al.*, 2008]. On the other hand, the passage of a strong stream such as the SAF or SACCF is generally associated with a chlorophyll-depleted band in satellite chlorophyll images, as will be seen later.

The spatial distribution of water properties over the Kerguelen Plateau (Figure 2) [*Park and Vivier*, 2011] is constrained by bottom topography, well reflecting the general circulation described in the literature [*Park et al.*, 2008c; *Park and Vivier*, 2011]. Here maps of subsurface water properties at 200 m depth, which is the representative core depth of the Winter Water south of the PF, illustrate the spatial distribution of subsurface waters of different origins. The SAF can be easily recognized by enhanced temperature and salinity gradients centered at 45°–46°S in the north of the Kerguelen Islands. It gradually shifts southward while energetically meandering in the downstream area. North of the SAF are warm, saline, and light waters of the subtropical origin (Figures 2a–2c). The Subantarctic zone between the SAF and Subtropical Front is practically nonexistent because these two fronts tightly merge in this particular region [*Park et al.*, 1993]. On the other hand, strong gradients in salinity and density within the Fawn Trough suggest the presence of the SACCF, although the subsurface temperature field does not reveal any noticeable gradient there. The most conspicuous feature between the SAF and SACCF is the cold, saltier, and denser Antarctic water propruding northwestward along the eastern escarpment extending as far north as the northeastern corner of the Kerguelen Plateau. The altimetric streamline marked as the PF (Figure 2d) demarcates such subsurface water, indicating the origination of this water from the Antarctic zone. The Polar Frontal zone refers to the region between the PF and SAF [*Nowlin and Klinck*, 1986] and is best characterized in our case by a well-developed and widespread subsurface salinity minimum (Figure 2b), which is consistent with the traditional definition of the SAF as the northernmost boundary where the subsurface salinity minimum descends rapidly below 400 m to form the Antarctic Intermediate Water [*Whitworth and Nowlin*, 1987; *Park et al.*, 1993].

The 2011 KEOPS2 cruise was carried out in the red rectangular area shown in Figure 2. It is probably the most extensive multidisciplinary oceanographic cruise ever conducted in the area. Although the gross features of the general circulation of the Kerguelen region have been known as mentioned above, the study area constitutes the most notorious sector of the Southern Ocean where a number of diverse definitions of the PF have been suggested in the literature, with an extreme difference in their geographical positions attaining as much as 10° of latitude, ranging from 46°S at 70°E [*Gilles*, 1994] to 56°S at 78°E [*Sokolov and Rintoul*, 2009], corresponding to our SAF and SACCF. For more background knowledge on the large-scale frontal circulation pattern and associated vertical structure of water masses in the Indian sector of the Southern Ocean across the Kerguelen Plateau, the reader is referred to *McCartney and Donohue* [2007] and *Roquet et al.* [2009]. A precise determination of the PF is critically important because the advective effect of
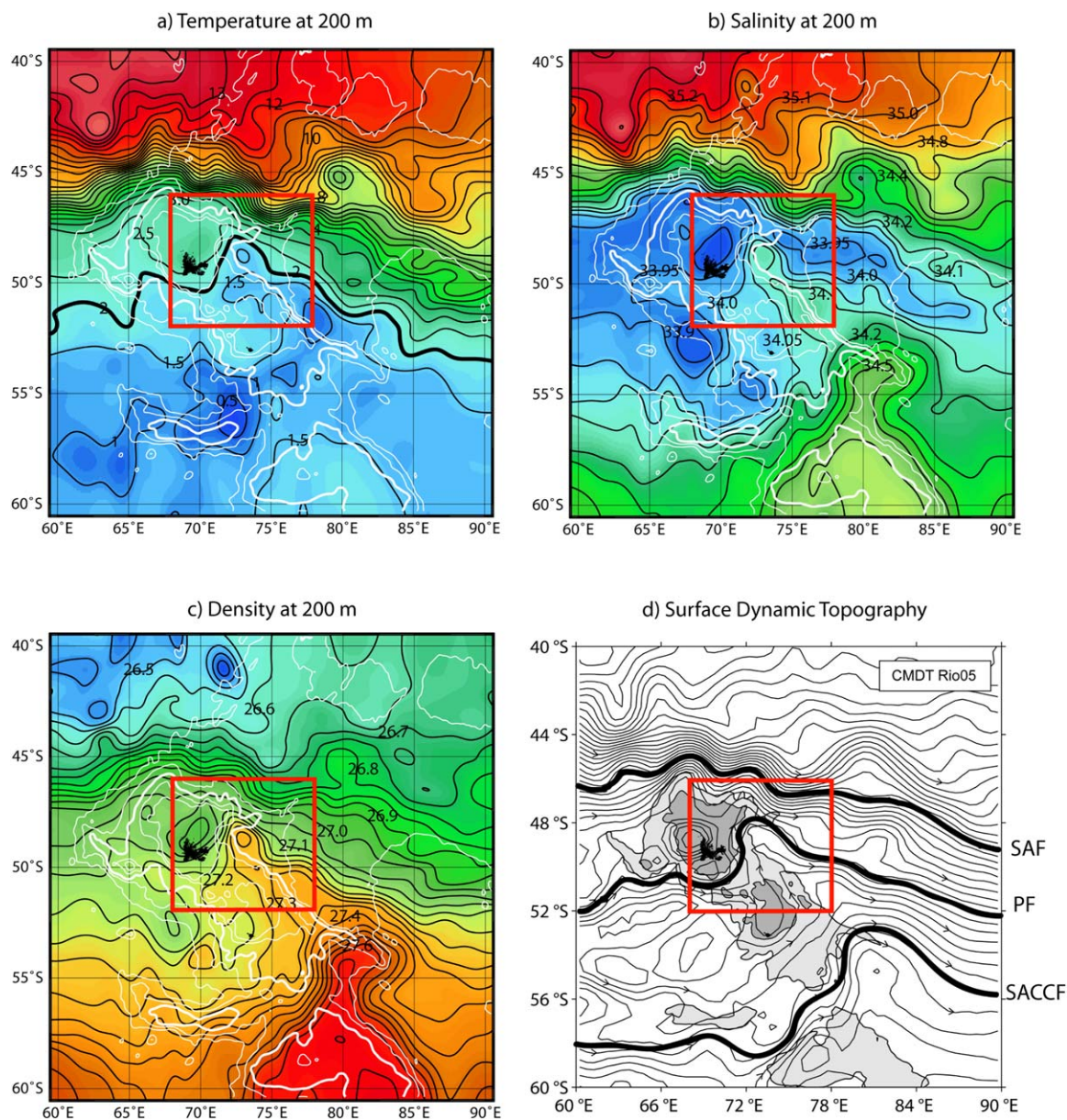
Figure 2. (a–c) Property distributions at 200 m and (d) an altimetry-derived mean surface dynamic topography in the Kerguelen region. Thick white lines in Figures 2a–2c represent the 2000 m isobath and thick black lines in Figure 2d indicate three major ACC fronts. The red rectangular area corresponds to the KEOPS2 cruise area that is presented in Figure 3. Adapted from *Park and Vivier* [2011].

iron from the plateau likely plays an important role in the annually recurrent bloom around the Kerguelen Islands [e.g., *Blain et al.*, 2007; *Bown et al.*, 2012], thus having a potential implication for the air-sea CO_2 flux and climate. In view of the recent increasing interest of the Kerguelen region for climate-related studies, the hitherto-proposed diverse locations of the PF in our study area appear to create great confusion [*Roquet et al.*, 2009], so it is time to erase this long-lasting ambiguity. Here we would like to determine an up-to-date climatological location of the PF around the Kerguelen Islands from all available quality-controlled hydrographic data and based on the widely accepted best criteria of the front, before validating the results in comparison with the extensive survey data from the KEOPS2 cruise.

Based on the in situ hydrographic and current measurements as well as drifters tracking data during the cruise, together with historical hydrographic data, satellite chlorophyll images, and altimetry-derived surface velocity fields, a precise analysis of the PF is conducted in relation to the distribution of surface/subsurface water masses, the temporal evolution of its frontal position, and associated frontal exchange of water
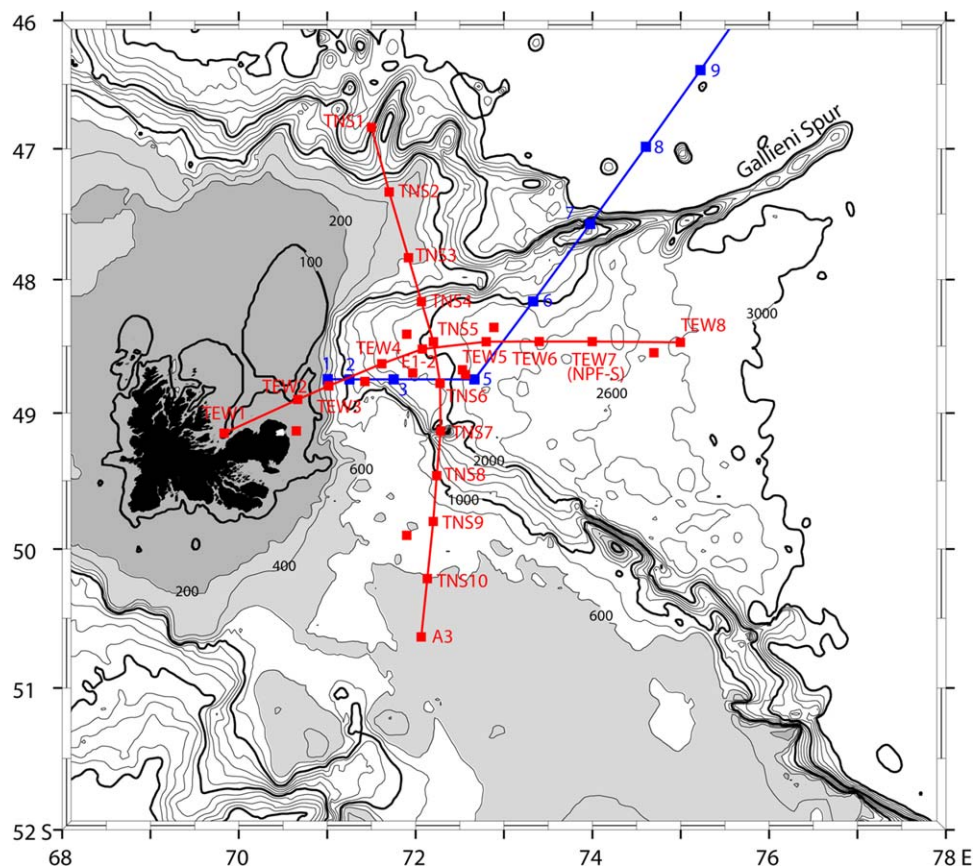
Figure 3. (a) Map showing the 2011 KEOPS2 CTD stations (red dots) on (or close to) two N-S and E-W transects (red lines) superimposed on the detailed bathymetry. The blue line represents the MAKER XCTD transect made in January 2011. Isobaths are every 200 m except for 100 m. The seabed shallower than 600 m (200 m) is lightly (darkly) shaded. Isobaths of 100 m and every 1000 m are thickened.

masses. A circulation schematic of surface/subsurface waters is also suggested based on artificial particle trajectories tracked from fine-resolution altimetric velocity time series fields.

2. Data

2.1. In Situ CTD and LADCP Data

The in situ hydrographic data used in this paper originate from the October–November 2011 KEOPS2 cruise carried out aboard the R/V Marion Dufresne in the northeastern plateau/slope area immediately east off the Kerguelen Islands (Figure 3). We used a total of 25 full-depth CTD (Conductivity-Temperature-Depth) profiles gathered using two sets of Sea-Bird SBE 9*plus* sensors (red squares in Figure 3). Many of these stations were reoccupied several times for shallow casts to have biogeochemical samplers and microstructure turbulence measurements. During CTD casts, horizontal current profiles throughout the water column were obtained from a pair of downward and upward looking RD Instrument 300 kHz lowered acoustic Doppler current profilers (LADCPs) attached to the rosette. The R/V Marion Dufresne was also equipped with two ship-borne acoustic Doppler current profilers (SADCPs): a "narrow band" 150 kHz and an "Ocean Surveyor" 75 kHz which provided horizontal currents as a function of depth in the first 300 m and 700 m, respectively.

These CTD/LADCP stations were mostly located on two near-perpendicular transects (red lines) in the area where the V-shaped continental slope changes its orientation from the southeast-northwest direction in the southeast of the Kerguelen Islands to the southwest-northeast direction at the northeastern corner of the Kerguelen Plateau. The latter connects with the Gallieni Spur, a narrow submarine ridge which separates the Kerguelen-Amsterdam passage to the north from the Australian-Antarctic Basin to the south. The north-south transect (TNS) cuts the shelf areas found southeast and northeast of the islands, which are separated by the deeper inner corner of the V-shaped slope. The southernmost station A3 is the reoccupation of the
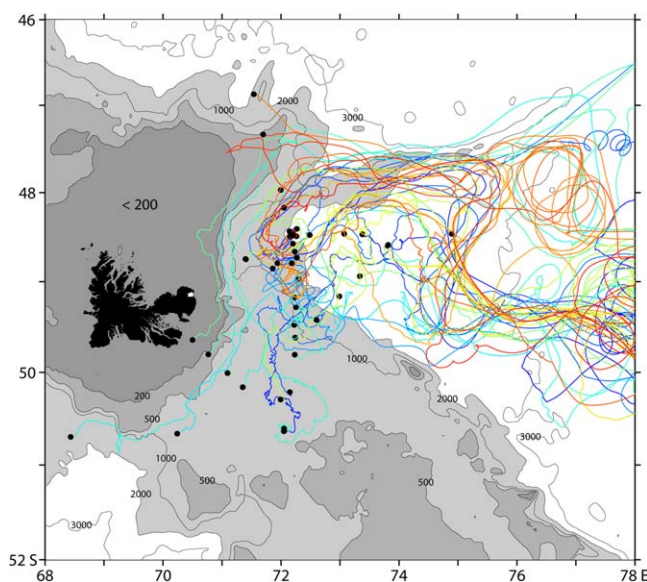
Figure 4. Trajectories of drifters deployed during the KEOPS2 cruise and satellite tracked until January 2012. Black dots represent the drifter launch points.

KEOPS1 time series station of the same label. The east-west transect (TEW) starts from the Baie de Baleiniers near the north central coast of islands, crosses the shallow shoal less than 100 m eastward closely along the axis of the V-shaped slope to the open ocean.

The CTD casts were supplemented with 22 rosette water samples for analysis of salinity and dissolved oxygen. The CTD sensors were calibrated before and after the cruise, and the post-cruise validated data for pressure, potential temperature, salinity, and dissolved oxygen are thought to be accurate within ± 3 dbar, $\pm 0.003°C$, ± 0.005 psu, and ± 0.005 ml l^{-1}, respectively. The LADCP measurements were processed following the method described by *Visbeck* [2002] and constrained in the surface layers by the SADCP measurements. The SADCP data were processed using the CODAS-3 software freely available at http://currents.soest.hawaii.edu/. The processing procedure is described in *Hummon and Firing* [2003].

2.2. Drifters Tracking Data

During the KEOPS2 cruise, a total of 48 drifters were deployed in October and November 2011. These drifters met the WOCE/SVP (World Ocean Circulation Experiment/Surface Velocity Program) standards and were designed to follow water motion at 15 m. An example of trajectories of drifters tracked until 11 January 2012 is shown in Figure 4. We used the drifters-derived velocity data together with those from altimetry to construct the realistic circulation pattern of the study area during the cruise period, which will be discussed in section 4.

2.3. Satellite Altimetry and Chlorophyll Concentration Data

The KEOPS2 cruise benefited from regionally optimized satellite products provided in quasi-real time by AVISO/CLS (Archivage Validation Interprétation des données des Satellites Océanographiques/Collecte Localisation Satellites) with support from CNES (Centre National d'Etudes Spatiales). These products include multisatellite altimetry-derived sea surface height anomalies at a 1/8° resolution (compared to 1/3° resolution of the standard AVISO product), a regional updated Mean Dynamic Topography, and 1/25° Chlorophyll Modis and Meris composite images. We have used the altimetric data for constraining the drifters tracking data for constructing the mean surface geostrophic current field during the cruise (section 4) as well as tracking artificial water particles seeded in the upstream of the study area to identify the pathways and sources of surface/subsurface waters advected into the study area (section 6). The high-resolution chlorophyll concentration images appear as an excellent marker of the fronts and filaments in our study area, so that they were used here as supporting evidence for the frontal circulation determined from the combined hydrography, altimetry, and drifters tracking data (section 4).

2.4. Historical Hydrographic Data

In order to better interpret the KEOPS2 observations within the general circulation context and to accurately determine the climatological PF location, we used all available historical and recent hydrographic data in the study area. These include not only conventional hydrographic data but also autonomous Argo float-derived CTD profiles. We also included still-unpublished XCTD (expendable CTD) data collected annually between 2011 and 2013 as part of the MAKER project, an IPEV (Institut Paul Emile Victor)-sponsored multi-year monitoring project in the Kerguelen area. The blue section in Figure 3 shows a part of the XCTD section
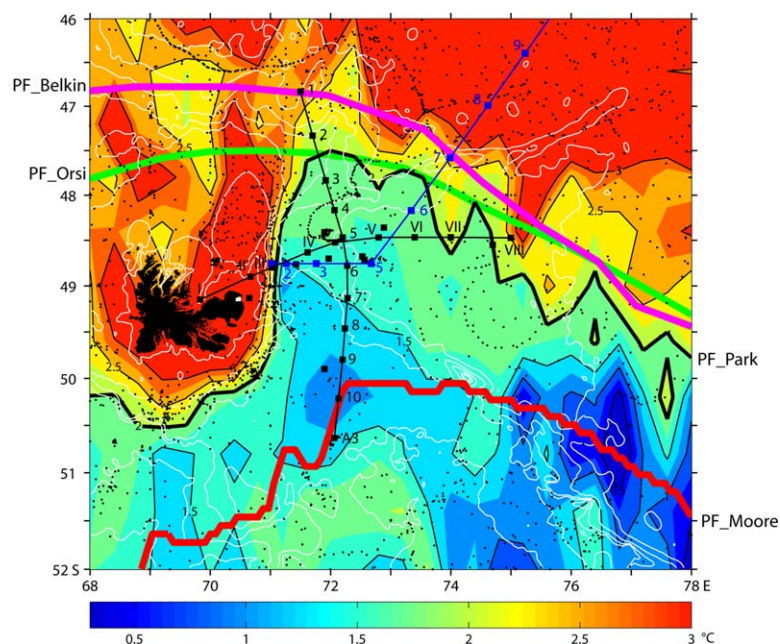
Figure 5. Temperature field at the subsurface temperature minimum layer. Small dots represent in situ data points. The 2°C isotherm corresponding to our PF (PF_Park) is shown by a thick black line. Also shown by colored thick lines are three PF locations suggested by other authors.

made in January 2011, which will be referenced in section 5 when interpreting the KEOPS2 CTD data in terms of cross-frontal exchange of water masses.

3. Determination of the Polar Front

3.1. An Up-To-Date Determination of the Climatological PF From Hydrographic Data

Before determining the exact location of the PF in the study area, it may be instructive to briefly recall the two key criteria of the front. The most critical definition of the PF is based on its hydrographic characteristics at the northernmost boundary of the Antarctic zone, which can be best characterized by the presence of the Winter Water, a subsurface water mass formed during the precedent winter season and residing underneath the summer mixed layer without changing much its initial winter characteristics. The most traditional definition accounting for this hydrographic feature corresponds to the northern limit of the subsurface temperature minimum (Tmin) of 2°C [*Botnikov*, 1963], which has been widely adapted in the literature [e.g., *Whitworth and Nowlin*, 1987; *Park et al.*, 1993; *Orsi et al.*, 1995; *Belkin and Gordon*, 1996, among others]. The second important criterion of the PF, though applicable equally to other fronts, relies on its dynamic characteristics such as a distinct band of strong currents or velocity shear associated with the baroclinic pressure gradient, large-scale information of which can be obtained from maps of dynamic topography from hydrography or altimetry. The ideal PF location should be the one that satisfies the above two hydrographic and dynamic criteria, although the former criterion is prerequisite. If only the latter dynamic criterion is taken into consideration, however, there is no guarantee that the front determined as such corresponds really to the PF because other fronts (e.g., SAF or SACCF) may equally satisfy that criterion [e.g., *Gilles*, 1994; *Sokolov and Rintoul*, 2009]. Sometimes, a distinctive meridional gradient of temperature has been used as a criterion, especially using the satellite sea surface temperature data [*Moore et al.*, 1999]. However, a similar precaution as for the above dynamic criterion should be kept in mind.

Figure 5 illustrates a map of subsurface Tmin determined in the 100–300 m depth range using all available historical and recent hydrographic data, including 1298 data points from CTD, 877 points from Argo floats, and 31 points from XCTD observations. The PF corresponding to the 2°C isotherm of Tmin is emphasized by a thick black line marked as PF_Park, which is compared with other definitions by *Belkin and Gordon* [1996], *Orsi et al.* [1995], and *Moore et al.* [1999], marked as PF_Belkin, PF_Orsi, and PF_Moore, respectively.

Consistent with some previous work [e.g., *Park et al.*, 2008c; *Park and Vivier*, 2011], the PF_Park separates the cold Winter Water (<2°C) of the Antarctic zone from the warmer Polar Frontal zone subsurface waters, rounding the Kerguelen Islands from the south along the inner slope south and east of the islands (Figure 5). It is noteworthy that no water colder than 2°C is found over the vast shallow (<200 m) shelf north of the Kerguelen Islands, where the coldest temperature ranging from 2.3°C to 3.3°C within the water column is observed near the bottom. An abrupt zonal discontinuity in Tmin occurs at ~71°E between the warmer (>3°C) shelf water north of the islands and the cold (<2°C)

Winter Water in the deep off-plateau area northeast of the islands, suggesting no direct zonal circulation connecting these two adjacent areas. The PF_Park here exhibits rather an abrupt northward deflection over a meridional distance over 300 km from its southernmost position (50°30′S, 69°E) south of the islands to its northernmost position (47°30′S, 72°E) at the northeastern corner of the Kerguelen Plateau, from which the front retroflects gradually back to the south. This northward deflection of the PF along the eastern slope is in good agreement with strong slope currents identified there from a systematic analysis of drifts of demersal longlines between their deployment and recovery positions for the Kerguelen Patagonian toothfish fisheries [*Park et al.*, 2008a].

In contrast, the PF_Orsi and PF_Belkin round the Kerguelen Islands from the north (not south), passing across the shallow shelf or along the northern slope, which are located farther north of the PF_Park by as much as 300–400 km, although they become much closer (within 50–100 km) to the PF_Park in the downstream area of the plateau. On the other hand, the PF_Moore is found farther south by 200–300 km relative to the PF_Park, passing through the much colder (<1.5°C) Winter Water. In summary, based on abundant historical and recent hydrographic data, the PF_Park provides a more detailed and up-to-date climatological location of the PF compared to those previously suggested in the study area.

One may wonder why the frontal positions north of Kerguelen of the PF_Belkin and PF_Orsi are so radically different from the PF_Park south of the islands, given the same hydrographic criterion (2°C Tmin) applied in principle to all three cases. Then, what is really represented by the PF_Belkin and PF_Orsi as compared to the PF_Park? Close reading of the relevant references [*Orsi et al.*, 1995; *Belkin and Gordon*, 1996] allowed us to unveil the potential causes that might have been responsible for the observed difference in frontal location. In the case of *Orsi et al.* [1995], the difference comes from the limited data they used. For example, in our study area, these authors used only two selected hydrographic sections found each west (66°E) and northeast (71°–76°E) of the Kerguelen Islands, with no data over the plateau south of the islands [Figure 2 of *Orsi et al.*, 1995]. In this case, there would have been no other alternative than drawing their PF across the shallow shelf north of the islands. On the other hand, in the case of *Belkin and Gordon* [1996], the circumstances are far more complex. In fact, these authors used all meridional sections available at that time, with lots of unpublished Russian data including those from fishery surveys, so that the data density over the plateau surrounding the Kerguelen Islands [Figure 2 of *Belkin and Gordon*, 1996] does not seem to raise any a priori problem. The most critical issue with these authors resides in their arbitrary choice of the 2.5°C Tmin criterion applied exceptionally to the Kerguelen region (60°–80°E), with the 2°C criterion otherwise, in order to favor the northern branch of the PF north of Kerguelen based on the argument like "*the conservation of potential vorticity that forces an equatorward deviation of the flow over shallowing depths*." They also tried to justify the exceptional choice of 2.5°C for the Kerguelen region by noting "*Taking into account the exceptionally low latitude of the PF in this area (up to 46°-47°S), this warming seems quite natural*." While the equatorward deflection over shoaling depths could be explained by the conservation of the barotropic potential vorticity (f/H) (where f is the Coriolis factor and H is bottom depth), it might not be an adequate parameter for describing the baroclinic shear flow within the subsurface Tmin layer where the baroclinic potential vorticity fN^2/g (where N^2 is the squared Brunt-Väisälä frequency and g is the acceleration due to gravity) should be rather appropriate [e.g., *McCartney and Donohue*, 2007]. The flow in this case is no more controlled by H but is a function of the isopycnal layer thickness, so the subsurface Tmin layer can flow freely over the plateau, except over depths much shallower than 300 m or so where the Tmin layer can be grounded. Furthermore, the thesis of warming of Tmin from 2°C to 2.5°C due to the northward deflection of the PF does not appear to be well grounded because there is no apparent heating source in the Tmin layer that is sheltered from the surface heating by a seasonal thermocline. By the way, it is also noteworthy to remark a doubtful Tmin showing an isolated, unusually cold core (T < 0.5°C, S ∼ 34.1 psu at 300 m at 47°S) tightly attached to the SAF at 46°S in the Akademik Shirshov cruise 5 section along 70°E [Figure 14 of *Belkin and Gordon*, 1996]. In our quality-controlled historical hydrographic data set, such a low temperature Tmin is only found to the south of 50°S along the northward branch of the Fawn Trough Current flowing along the eastern escarpment of the Kerguelen Plateau [see Figure 5; *Park et al.*, 2008c; *Roquet et al.*, 2009], which has never been observed north of the Kerguelen Islands (compare the above cold core T/S point (0.5°C, 34.1 psu) with any T-S diagram shown in the present paper).

We will examine below whether the PF_Park, which will be referred hereafter simply as the PF, also satisfies the second dynamic criterion of the front, i.e., concentration of strong currents.
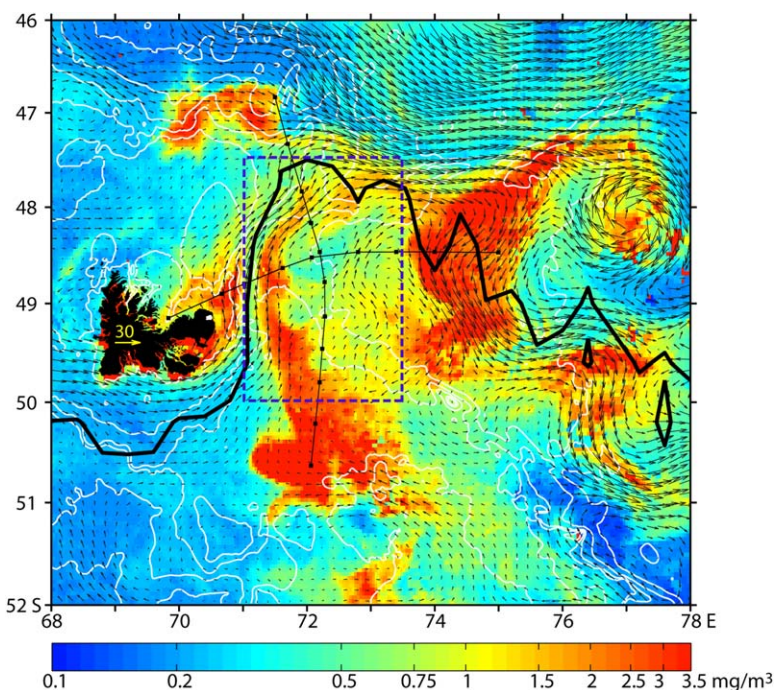
Figure 6. Mean surface velocity field during the KEOPS2 cruise constructed from the combined data sets of drifter-derived currents within the dashed rectangular area and altimeter-derived currents outside the rectangular area. The velocity scale for 30 cm s^{-1} is shown on the Kerguelen Islands. See the text for the details of the methodology. Composite chlorophyll images (color shading) during the KEOPS2 cruise, the two transects (thin lines), and the PF_Park (thick black line) from Figure 5 are superimposed.

3.2. Mean Surface Geostrophic Velocity Field From Drifters and Altimetry

In order to get the reliable information on a large-scale surface circulation pattern in the study area during the cruise, we have synthesized all drifters-derived near-surface velocity vectors obtained during the cruise period within the dashed rectangular area of Figure 6 and mean altimetry-derived surface velocity field for the domain outside the rectangular area. The drifter-derived velocity data represent the composite of individual vectors for the 1 month period from 19 October to 19 November, while the altimetric velocities have been averaged over the same period at each altimetric grid points. These combined data sets have undergone an optimal interpolation on a fine grid (1/20° lat × 1/12° lon) based on a stream function method to generate a nondivergent geostrophic velocity field [*Bretherton et al.*, 1976] (Figure 6). In order for further increasing the credibility of these velocity fields, the composited chlorophyll concentration (color shading) over the same period is superimposed.

It is remarkable that both the velocity and chlorophyll fields follow coherently the hydrography-derived PF location (thick black line). This is most clear for the northward deflecting PF along the eastern escarpment east of the Kerguelen Islands and its eastward turning at the northeastern corner of the Kerguelen Plateau. The PF here is associated with a concentrated strong flow that is accompanied with a narrow band of clear-cut chlorophyll-poor waters advected from the far upstream in the southwest of the islands. Immediately north of the PF are the southward bending strong currents along the base of the northern escarpment, accompanied with a band of chlorophyll-poor waters. When Figure 6 is compared with Figure 2, it is not difficult to recognize that these southward bending strong currents correspond in effect to the SAF. Merging of the PF and SAF, with the plume-like flow emanating from the shallow Kerguelen shelf being sandwiched between them, occurs along the northern flank of the Gallieni Spur. The southward retroflecting PF in the eastern half of the study area is associated with highly meandering, much stronger and broader southward flow, probably because of the inclusion of the SAF waters. This southward bending PF generally follows the meandering southward flow but the correspondence between the two features is significantly less compared to the northward flowing PF in the west. This is probably related to highly time-varying energetic mesoscale meanders frequently observed in the eastern half of the study area, as will be seen later. Also remarkable here is that the strong flow is mostly associated with well-
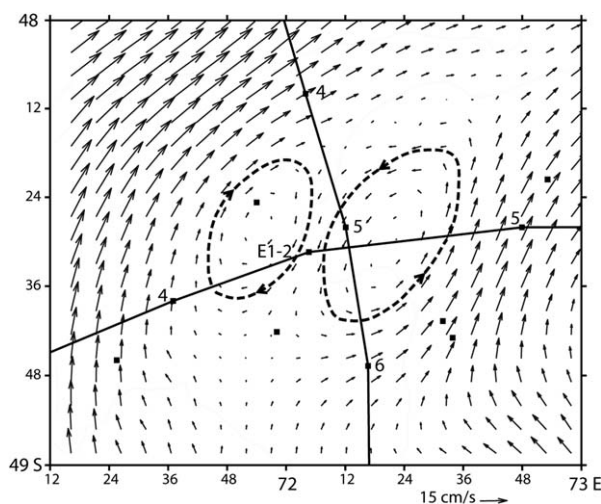
Figure 7. Zoom of the drifter-derived velocity field in the central part of the dashed rectangular area of Figure 6a. Two dashed ellipses are superimposed to help detecting a twin-like secondary circulation pattern in the stagnant central part of the area.

developed high-chlorophyll patches, in great contrast to the chlorophyll-depleted band along the axis of the western PF.

Finally, we remark that there appears some noticeable secondary inner circulation, showing a dominant northward flow in the eastern half of the rectangular area. Another remarkable feature is observed in the central part where the N-S and E-W transects cross. Here the drifters solution reveals a nearly stagnant feature associated with a local minimum in chlorophyll. As this central part of the study area had been considered during the cruise as the key area for repeating a number of biogeochemical stations, a zoom of the detailed local velocity field is shown in Figure 7. There is clearly a weak small-scale (<50 km) anticyclonic eddy detached from the northward branch of flow (at 72°40′E) coming from the southern shelf (Figure 6). It can be also noticed that a less significant cyclonic feature is sandwiched between the just-mentioned anticyclonic eddy and the strong northward flowing PF west of 71°30′E. Although it may not be so significant in terms of dynamics, the weak southward flow associated with this twin-like circulation pattern can affect significantly water properties at nearby
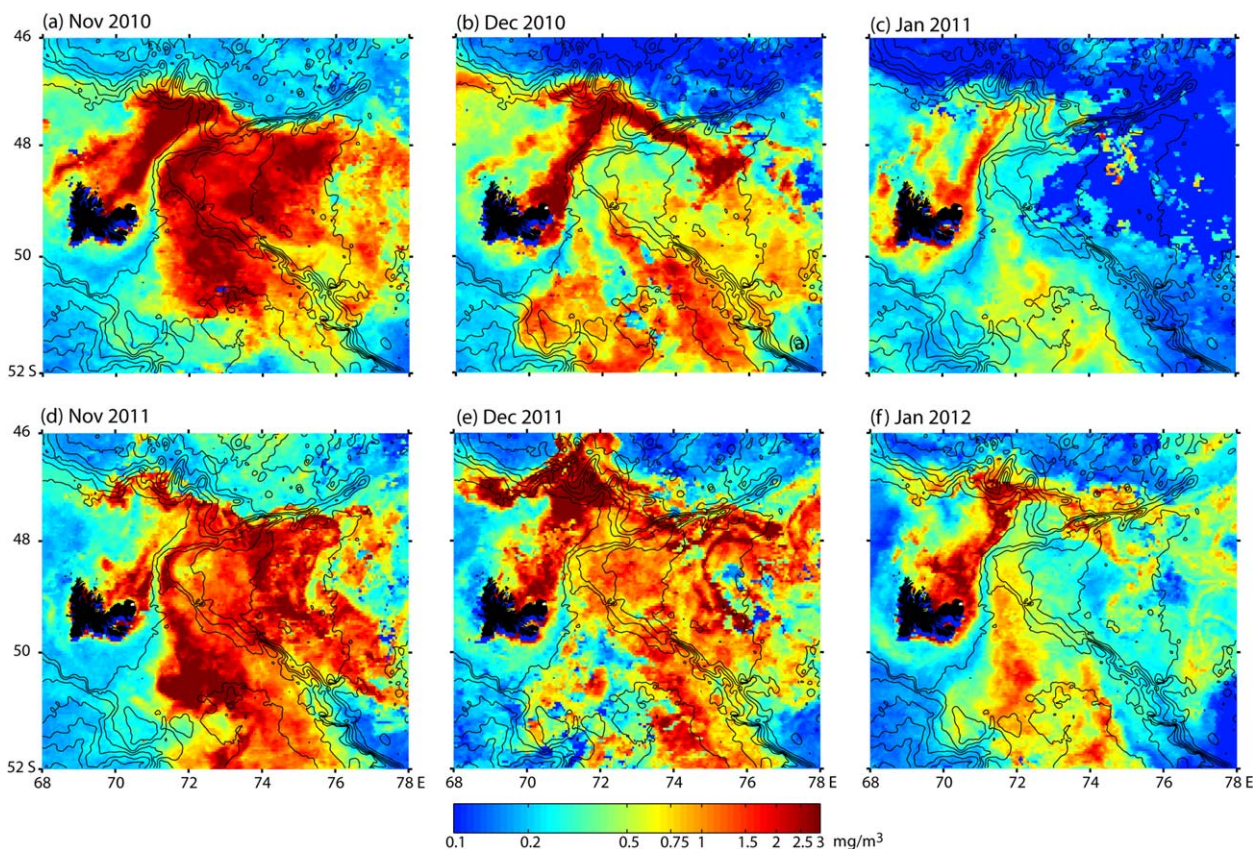

Figure 8. Monthly composite chlorophyll images for November through January of 2010/2011 and 2011/2012.
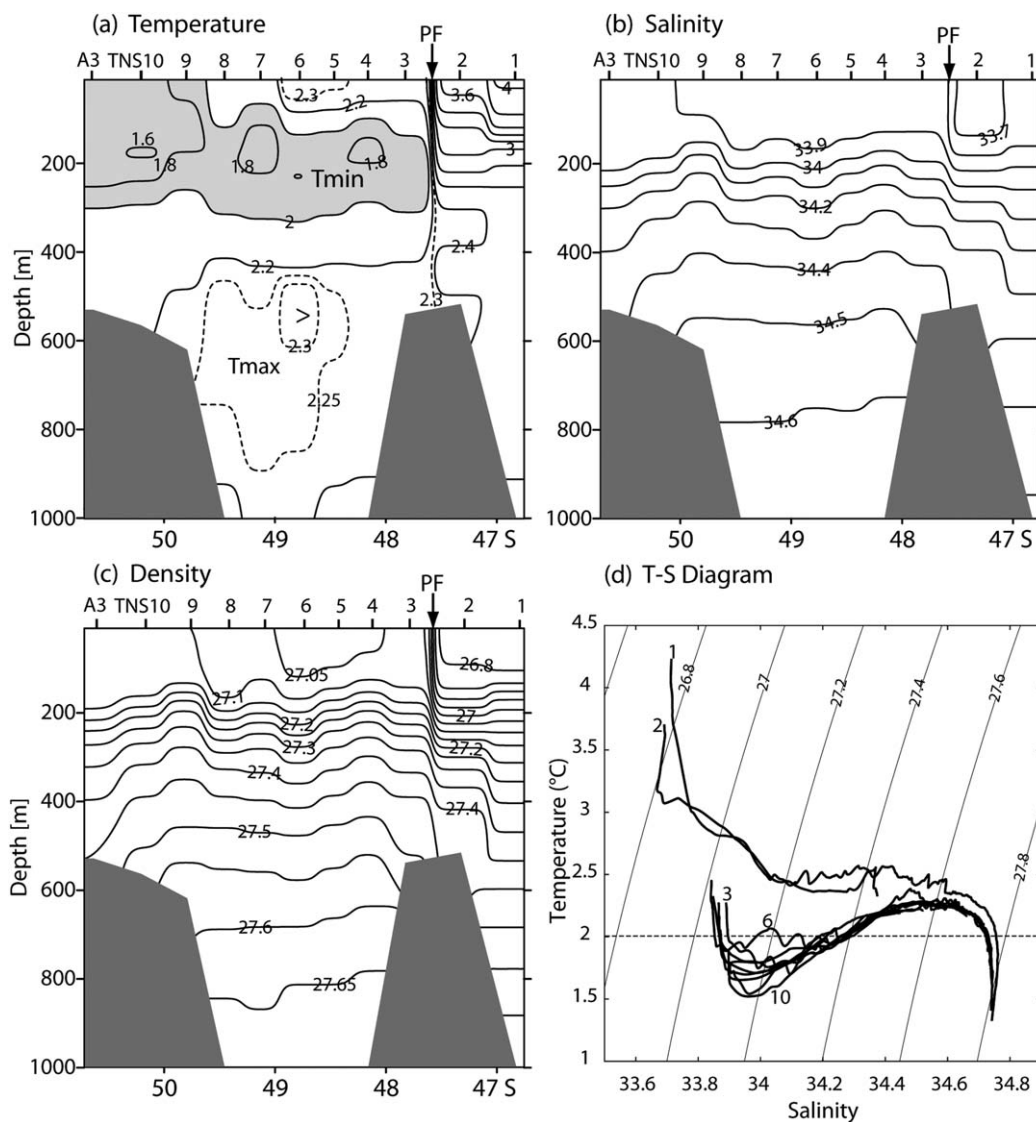
Figure 9. (a–c) Property sections of the upper 1000 m along the N-S transect during the KEOPS2 cruise and (d) the corresponding full-depth T-S diagram. The contour interval in Figures 9a–9c is 0.2°C for potential temperature except for dashed supplementary isotherms, 0.1 psu for salinity, and 0.05 kg m^{-3} for potential density. The area with a temperature less than 2°C is shaded in Figure 9a. In Figure 9d, some selected station numbers are indicated near the corresponding T-S curves.

stations. It is also likely that this central part corresponds to the latest arrival of water particles originating from the shallow plateau, which may explain the retarded bloom there compared to the outer boundary of the PF circulation system (see Figure 6).

3.3. Chlorophyll Concentration as an Excellent Marker of the PF

The spatial distribution of chlorophyll concentration during the cruise period is remarkably coherent with the PF location especially in the western half of the study area. More complete information on the chlorophyll concentration can be seen in monthly composite maps for the late spring to early summer period of 2010/2011 and 2011/2012 (Figure 8). Temporally, the spring bloom over the study area peaked in November and faded gradually through December and January, although the degree of fading depends on the place and year. Spatially, the chlorophyll-rich plume from the shallow shelf north of the Kerguelen Islands persisted until January especially in 2012, while the one within the inner part of the cyclonically meandering PF in the off-plateau completely disappeared. The persistent chlorophyll plume emanating from the northern Kerguelen shelf compared to the earlier fading bloom in the off-plateau area makes a clear distinction of the outer boundary of the PF, as most clearly evident in Figures 8b and 8f. Moreover, the northward
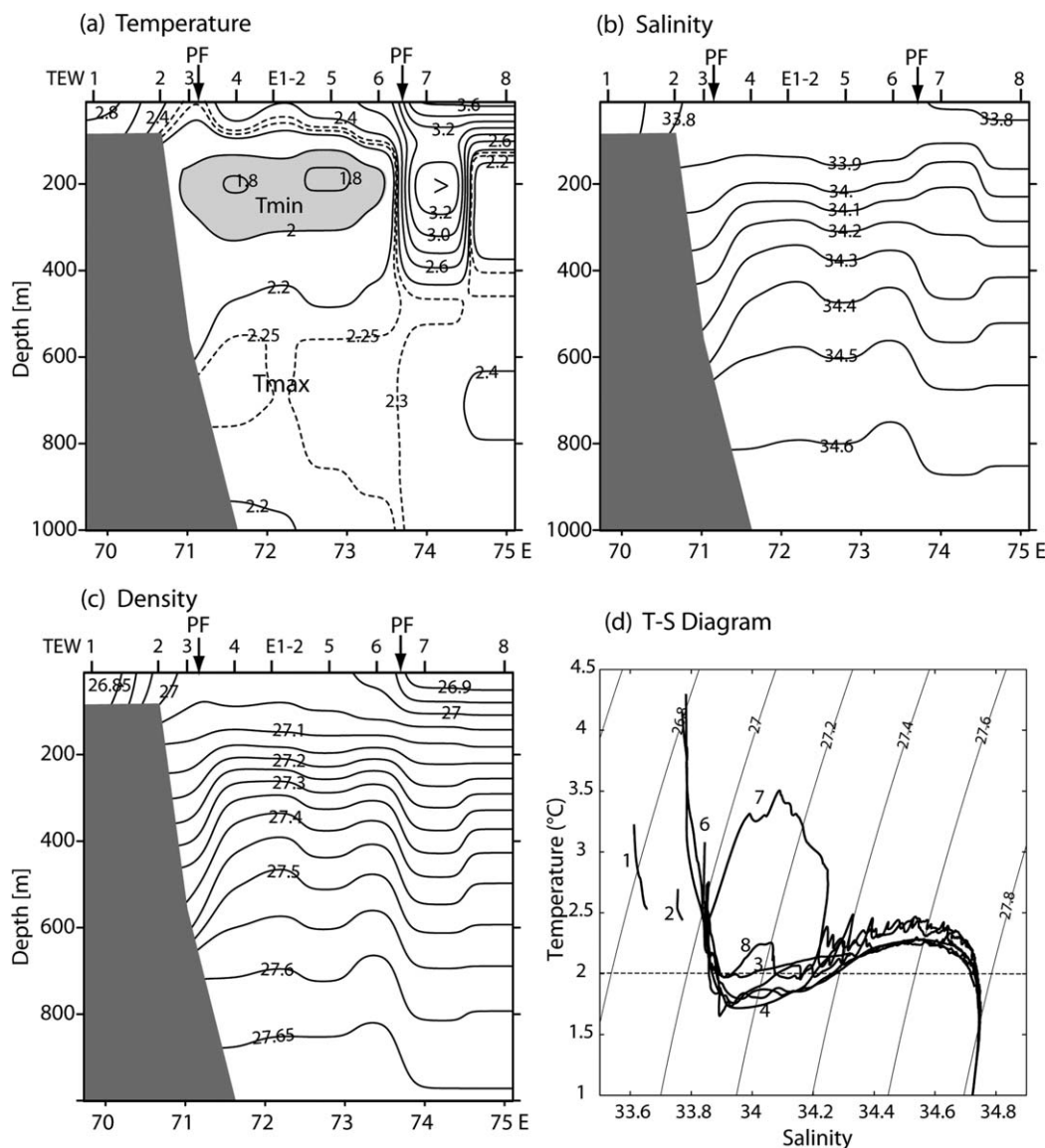
Figure 10. Same as Figure 9, except for the E-W transect.

deflecting PF immediately east of the islands and its upstream signature in the south of the islands are obvious in all monthly maps by the presence of a band of local chlorophyll minimum originating from the chlorophyll-poor upstream waters southwest of the islands. Consequently, the chlorophyll concentration can be efficiently used as an excellent marker of the PF location in our study area, which is also remarkably coherent with the results obtained from hydrography and velocity fields (Figures 5 and 6).

4. In Situ Observations of the PF During the KEOPS2 Cruise

4.1. Property Sections and Water Mass Analysis

The vertical property sections of the upper 1000 m and the full-depth T-S diagram along the N-S and E-W transects are shown in Figures 9 and 10, respectively. Along the N-S transect, an abrupt property change in the surface layer appears between TNS2 and TNS3, which coincides also with the northern limit of the Tmin of 2°C at 200 m (Figure 9a), indicating undoubtedly the existence of the PF there. This PF from in situ hydrographic data is in excellent agreement with its climatological position seen in Figure 5. It also agrees well with the PF_Orsi but completely disagrees with the PF_Belkin and PF_Moore. To the north of the PF, on the other hand, no water colder than 2°C appears and the surface water becomes distinctively warmer

(T > 3°C), fresher (S < 33.8), and lighter (σ_t < 26.8 kg m^{-3}) than that south of the PF. This discontinuity in property distribution across the PF is much clearer in the T-S diagram (Figure 9d) which shows two different types of T-S relationships between the stations north of the PF (TNS2 and TNS1) and those south of the PF, indicating different pathways or origins of waters. To the south of the PF, the Winter Water is clearly seen by a well-defined Tmin between 1.5 and 2°C, with a mean salinity around 34.0 and a mean potential density of 27.2 kg m^{-3}. At stations southeast of the Kerguelen Islands (TNS9, TNS10, A3), the water colder than 2°C reaches the surface, while at further northern stations it resides below the surface mixed layer (Figure 9a), suggesting that the Winter Water there must have been advected from the south rather than formed in place. The coldest Winter Water on the transect is found at TNS10, consistent with the climatology (Figure 5), which suggests that the major pathway of the northward advection of the Winter Water formed in the Antarctic zone south of the Kerguelen Islands passes close to TNS10.

Also, we observe at ~700 m a subsurface temperature maximum (Tmax) or the Upper Circumpolar Deep Water having a representative potential density of 27.6 kg m^{-3} (see Figure 9d). This Tmax water must have come either from the south through the Fawn Trough or from the north through the Kerguelen-Amsterdam passage because the shallow topography of the northern Kerguelen Plateau prevents such a deep water mass from directly overpassing the plateau. It is interesting to note that the northernmost extent of the Tmax of 2.3°C coincides with that of the Tmin of 2°C (Figure 9a), thus also marking the PF location. In this sense, TNS6 is atypical, showing an isolated Tmax warmer than 2.3°C centered at ~550 m, indicative of an influence by the water north of the PF. This is further supported by slightly warmer waters at the surface and in the Tmin layer at TNS6 compared to surrounding stations.

Along the E-W transect (Figure 10), the Winter Water (having a core temperature < 2°C near 200 m) is confined between TEW3 and TEW6. This feature together with a strong vertical shear implied by steeply sloping isopycnals seen in the potential density section (Figure 10c) permits us to place the PF in the vicinity of these two stations. This Winter Water is believed to have been advected from the southeast of the Kerguelen Islands as discussed. On the other hand, two shallow (~80 m) near-coastal stations located north of the Kerguelen Islands (TEW1, TEW2) are clearly distinguished from other stations especially by their very low salinity (33.6–33.8) and low density (<27.0 kg m^{-3}), with a relatively high bottom temperature of about 2.5°C. The T-S diagram in Figure 10d suggests that the waters at off-plateau stations have no apparent relationship with those at nearshore stations, further justifying the northward flowing PF located near TEW3. The southward retroflecting eastern PF is found between TEW6 and TEW7 where there appears a sharp eastward transition toward a warmer, fresher, and lighter water at the surface. The PF here also coincides with the Tmax of 2.3°C, as also discussed. However, the most uncommon feature observed at TEW7 is an isolated subsurface warm core (>3.2°C) centered at 200 m, which is in stark contrast with the more eastern station TEW8 where the subsurface water characteristics are close to those at TEW6. This abnormal feature at TEW7 is clearly indicated in the T-S diagram by a spectacular along-isopycnal intrusion of warm water (<3.5°C) in the Tmin layer (Figure 10d), which is likely associated with the frontal exchange with the warmer and saltier subsurface water associated with the SAF. This frontal exchange will be further discussed in section 5.

These two PF positions identified on the E-W transect during the KEOPS2 cruise are in good agreement with the climatology in Figure 5, suggesting that the PF location in the study area is relatively stable in time, except perhaps in its eastern, southward bending segment. The climatological PF also gives evidence of a southward protrusion of warmer Polar Frontal zone water at TEW7 and TEW8 and a northward protrusion of colder Antarctic zone water in between these two stations. This is likely related to highly time-variable mesoscale meandering of flow, which will be discussed in section 5. Note finally that the PF locations proposed by others (PF-Orsi, PF_Belkin, and PF_Moore) do not cross the E-W transect, while our updated PF confirms the cyclonic meandering of the PF in the off-plateau area east of the Kerguelen Islands.

4.2. Velocity Sections and Volume Transport

Figure 11 presents the LADCP velocities perpendicular to the N-S and E-W transects together with corresponding cumulative volume transports (top figures). Note that the LADCP data have been previously corrected for tidal currents estimated from regional high-resolution TUGO model developed for the south Indian Ocean [*Testut et al.*, 2012]. Also, in order to improve the velocity and transport estimation within the unresolved bottom triangle over a sloping bottom, the velocity profiles have been linearly interpolated on a
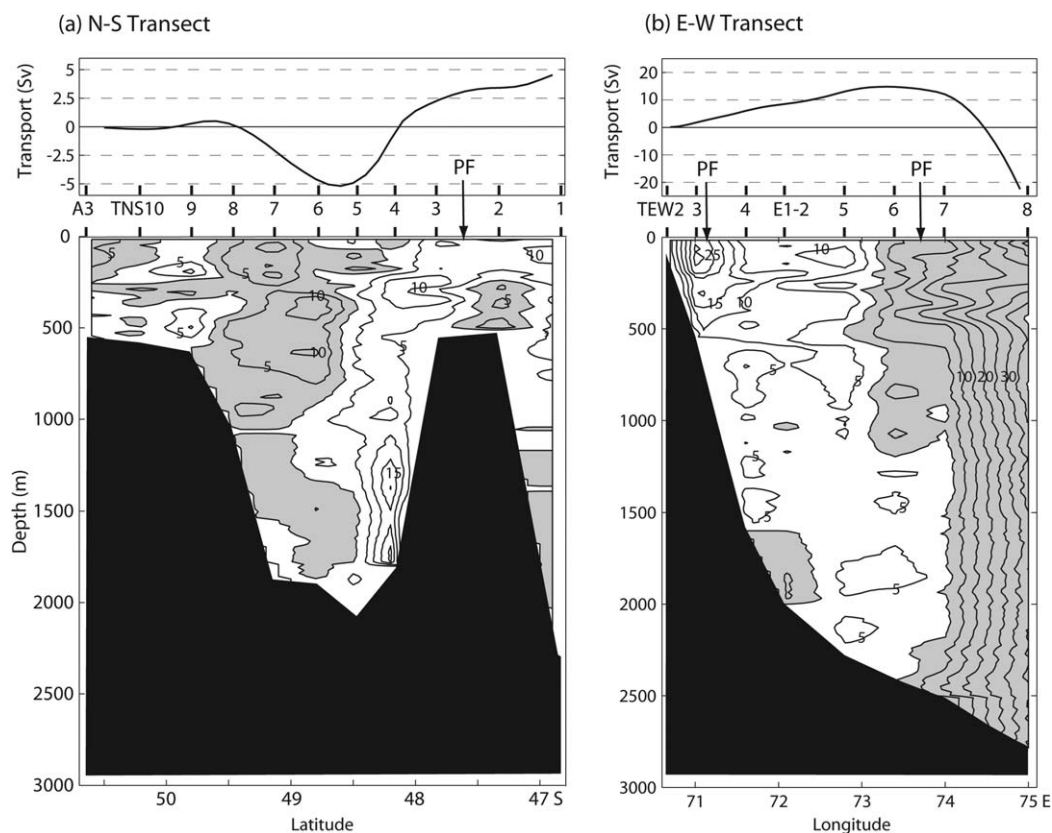
Figure 11. Vertical section of velocities (cm s^{-1}) perpendicular to (a) the N-S transect and (b) the E-W transect. The cumulative transport (Sv) on each transect is given in the top figures. The contour interval is 5 cm s^{-1} and the gray shaded areas correspond to westward velocities in Figure 11a and southward velocities in Figure 11b.

fine grid of 0.1° in latitude or longitude and 16 m in vertical, with zero velocities set on grid points below the bottom. Across the N-S transect (Figure 11a), a broad and weak (<12 cm s^{-1}) westward flow is observed between TNS8 and TNS6 in most of the water column, carrying a transport of 5 Sv over the southern V-shaped slope. On the other hand, the major eastward flow associated with the PF is tightly attached to the northern slope between TNS5 and TNS3, carrying a transport of 7 Sv. In particular, the strongest bottom-intensified eastward flow up to 20 cm s^{-1} is observed at TNS4, about 60 km south of the PF. In contrast, the eastward flow to the north of the PF is rather weak throughout the water column or even reversed in direction in the near-bottom layer, carrying only a minor transport of 1.5 Sv. This confirms that the PF_Belkin, which passes through TNS1, does not well represent the PF in this area. Similarly, the PF_Moore, which passes through TNS10 and A3 (Figure 5), is not associated with any remarkable eastward flow, but is rather associated with a weak westward flow less than 6 cm s^{-1} in the upper 200 m layer.

Across the E-W transect (Figure 11b), a strong northward flow up to 30 cm s^{-1} is concentrated at TEW3 where the PF is located nearby. The transport associated with this northward PF between TEW2 and TEW4 is 6 Sv, in good agreement with the previous ad hoc estimate by *Park et al.* [2009]. To the east of TEW4, a weak northward flow is prevalent throughout the water column until the midst of TEW5 and TEW6. In contrast to a roughly equivalent-barotropic structure to the west of TEW5, TEW6 and TEW7 reveal a clear baroclinic structure, with a moderate southward flow less than 20 cm s^{-1} in the upper 1200 m and a weak northward flow less than 7 cm s^{-1} below 1200 m. At TEW8, the strongest southward flow up to 35 cm s^{-1} exhibiting a nearly barotropic structure is observed. The cumulative transport from TEW2 (where the western PF begins to appear) reaches to a maximum of 15 Sv northward at TEW6, decreases significantly to the east of TEW7, and becomes 22 Sv southward at TEW8, with the zero transport line in the midst of these two easternmost stations. The southward PF was observed at 73°40′E during the cruise (according to hydrography), about 60 km west of this zero cumulative transport, although its position may vary somewhat depending on the meandering phase of the front. We interpret that the maximum cumulative transport of 15 Sv is
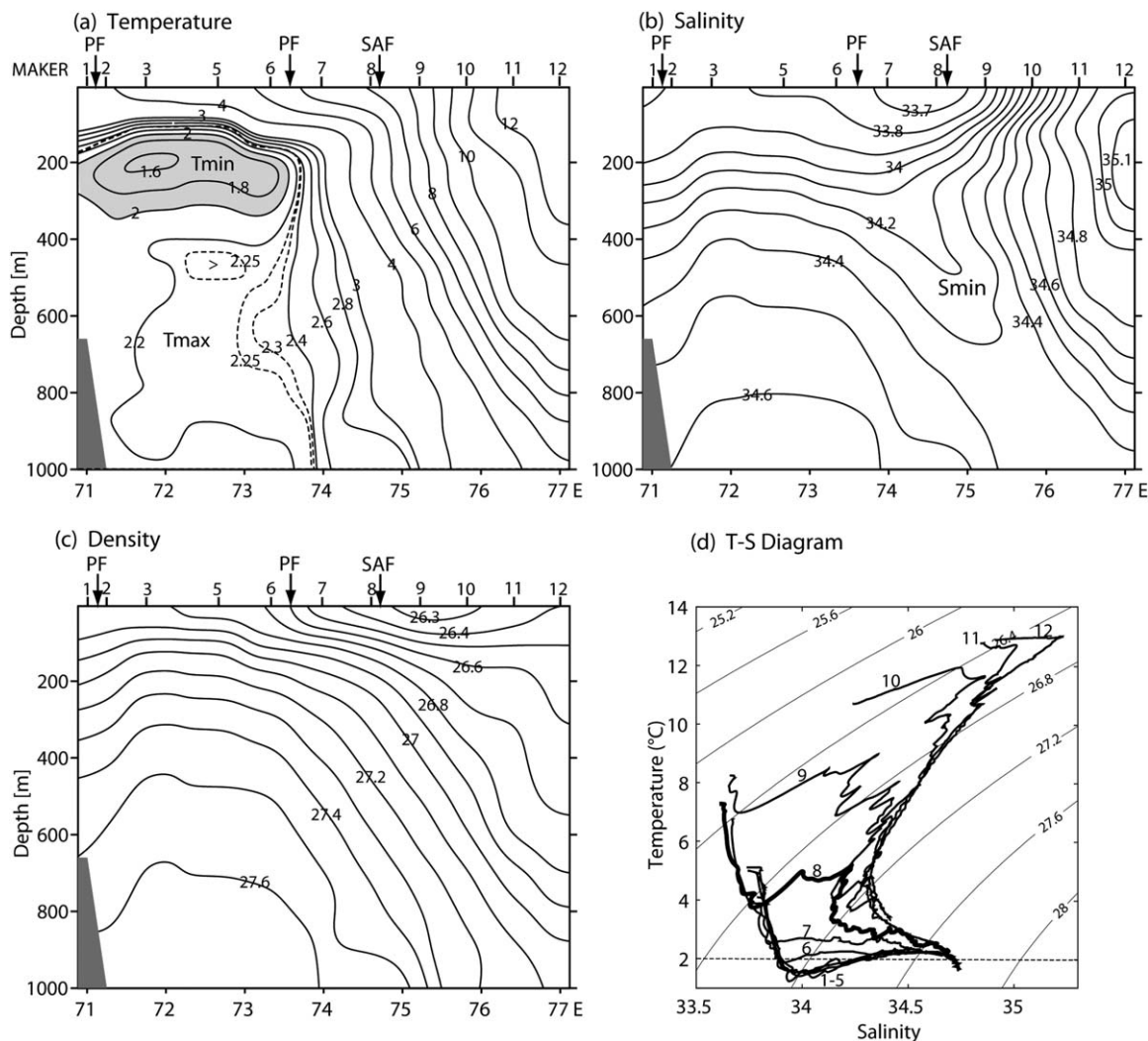
Figure 12. Same as Figure 9, except for the MAKER XCTD transect shown in Figures 3 and 5.

the total northward transport associated with the cyclonically circulating PF system of the area, including 6 Sv associated with the northward PF attached to the inner slope shallower than 1500 m west of TEW4, suggesting that the remaining 9 Sv should travel over the deeper outer slope. The net southward transport of 22 Sv at TEW8 may suggest that the southward PF here is tightly merged with a southern branch of the SAF carrying the same transport and bending southward across the Gallieni Spur (see Figure 6).

5. Temporal Variability of the Frontal Circulation

An abnormal warm core in the temperature minimum layer at TEW7 has been discussed in the previous section (Figure 10). This abnormal feature disappears completely when station NPF-S was reoccupied 6 days later. In order to understand this change in vertical property distribution in terms of temporal variability of the frontal circulation, we first examine the property sections in the upstream area from the January 2011 MAKER XCTD transect (Figure 12). The geographical positions of the XCTD stations up to station 9 are given in Figure 3. The PF crossed twice this transect: first, between stations 1 and 2, consistent with the observations on the KEOPS2 E-W transect and climatology (see Figure 5), and then between stations 6 and 7 across the Gallieni Spur, also consistent with the climatology. The SAF, which marks an abrupt deepening below 400 m of the subsurface salinity minimum to form the Antarctic Intermediate Water, can be placed near station 8, which coincides also with the surface salinity minimum (Figure 12b). The PF and SAF here are separated by 140 km only, which constitutes probably one of the closest convergence zones of the two fronts in
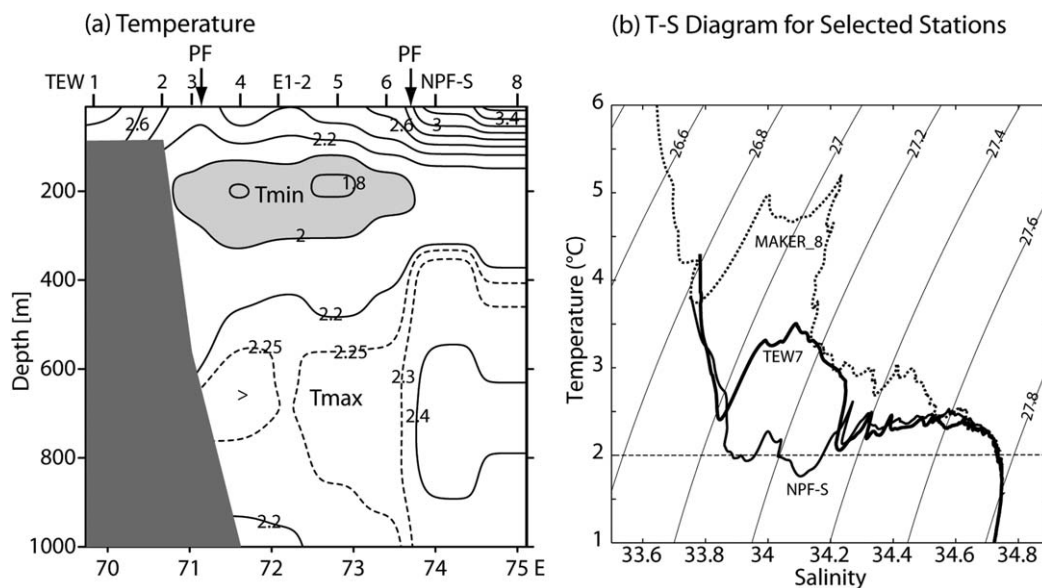
Figure 13. (a) Same as Figure 10a, except for NPF-S that is the repeated station of TEW7 6 days later. (b) Comparison of T-S curves at NPF-S, TEW7, and the MAKER XCTD station 8.

the Southern Ocean. North of station 9 is the Subtropical zone, whereas the Subantarctic zone here is practically nonexistent due to a tight merging of the SAF and Subtropical Front [*Park et al.*, 1993].

Figure 13a is the temperature section on the E-W transect, which is same as Figure 10a except that the CTD measurements at TEW7 are replaced by the repeated measurements noted as NPF-S. The abnormal subsurface warm core observed a week before at the same place (TEW7) is completely absent now, and the transition of subsurface temperature minimum across the PF is much more gradual compared to that in Figure 10a. Comparison of T-S curves at NPF-S and TEW7 in Figure 13b indicates that the two stations exhibit nearly same T-S relationships in the water column except in the Tmin layer centered at the potential density of 27.2 kg m^{-3}. In this Tmin layer, the T-S curve at NPF-S straddles the 2°C isotherm due to its proximity to the PF, while the T-S curve at TEW7 approaches closely to that of the MAKER XCTD station 8 placed near the SAF (Figure 12). This suggests that prior to the occupation of TEW7, a southern branch of the SAF must have flown so close to TEW7 that a cross-frontal injection or double-diffusive intrusion [e.g., *Ruddick and Turner*, 1979] of warm and saltier subsurface water associated with the SAF could occur. This indicates also highly time-varying frontal circulation of the area, which will be examined below.

In order to see the temporal variability of the frontal circulation associated with the southward retroflecting PF in the eastern half of the study area, three selected snapshots of altimetric surface currents are shown for the period before, during, and after the occupation of TEW7 in Figures 14a, 14b, 14c, respectively. In all maps, the northward flowing PF along the inner slope east of the Kerguelen Islands is visible by a band of moderate northward flow. The SAF is associated with the anticyclonically curving strongest flow north of the Gallieni Spur. Recall that on the MAKER XCTD transect (blue line), we have placed the SAF near station 8 and the PF between stations 6 and 7 (see Figure 12). This strong convergent flow between the SAF and PF becomes diverging into three branches to the east of 75°30′E; the main northernmost branch, which is most likely associated with the SAF core, bends northeastward along the Gallieni Spur; the second branch flows eastward crossing the spur and bends southward to form an energetic cyclonic eddy (centered near 48°S, 77°E); the third southernmost branch, which is closest to the PF, bends southward after crossing the spur at 75°30′E. These are quasi-permanent features, however, the downstream flow of the third branch is a noticeable time-varying meandering pattern (see dashed red lines).

Three distinct flow patterns associated with the eastern PF appear in Figure 14. About a week before the occupation of TEW7, the third southernmost branch executed an abrupt westward U-turn at 48°S, 76°E to flow westward before retroflecting anticyclonically just west of TEW7 to flow southeastward (Figure 14a). During the occupation of TEW7, the above S-shaped meander broke down and was short-circuited by two separate branches (Figure 14b); an upstream southward branch cutting the MAKER XCTD transect between
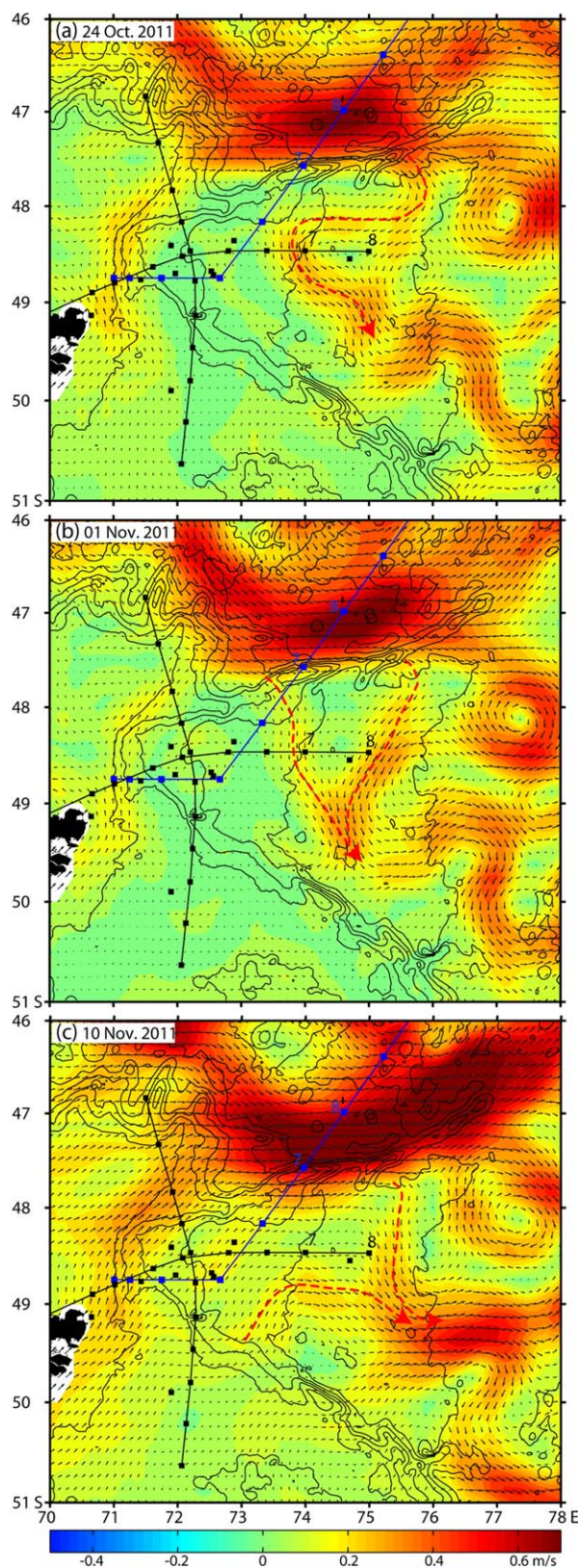
Figure 14. Snapshots of altimetric velocity field (a) 8 days before and (c) 9 days after (b) the occupation of TEW7. Arrows are velocity vectors and the color shading represents the velocity intensity. Dashed red lines are superimposed for clarifying the time-varying meandering PF.

stations 6 and 7 and the KEOPS2 E-W transect between TEW6 and TEW 7, similar to what observed in Figures 12 and 10, and an eastern southwestward branch passing just east of TEW8. The abnormal subsurface warm core observed at TEW7 is most likely related to the remnant SAF subsurface water previously advected into the vicinity of TEW7 by the S-shaped meander shown in Figure 14a (red dashed line). The frontal circulation changed continuously, and after 9 days since the occupation of TEW7 (Figure 14c), there appeared a near zonal flow south of the E-W transect in addition to a southward branch originating from the Gallieni Spur and passing just east of TEW8. The reoccupied station NPF-S, which was made a week after TEW7, did not reveal any abnormal feature (see Figure 13), probably because the subsurface warm core previously observed at TEW7 must have been swept away by the above-mentioned near zonal flow. Consequently, the exact location of the PF in the eastern half of the study area should vary substantially due to continually evolving meandering flow, which may also favor the intermittent cross-frontal exchange with subsurface waters of the SAF origin.

6. Summary and Discussion

We have determined an up-to-date location of the PF around the Kerguelen Islands from hitherto-accumulated abundant historical and recent hydrographic data according to the traditional definition of the front following *Botnikov* [1963], i.e., the northern limit of the subsurface Tmin of 2°C. This hydrography-derived climatological PF location has been systematically validated against the high-quality CTD/LADCP measurements and the satellite tracking of 48 surface drifters deployed during the recent KEOPS2 cruise. We have shown that the northern limit of the subsurface Tmax of 2.3°C marks equally well the PF. Further validation has been successfully conducted against satellite chlorophyll images and altimetry-derived velocity fields. All these in situ and satellite data sets confirm our climatological PF with a high degree of credibility, suggesting a stable geographical location of the contemporaneous PF
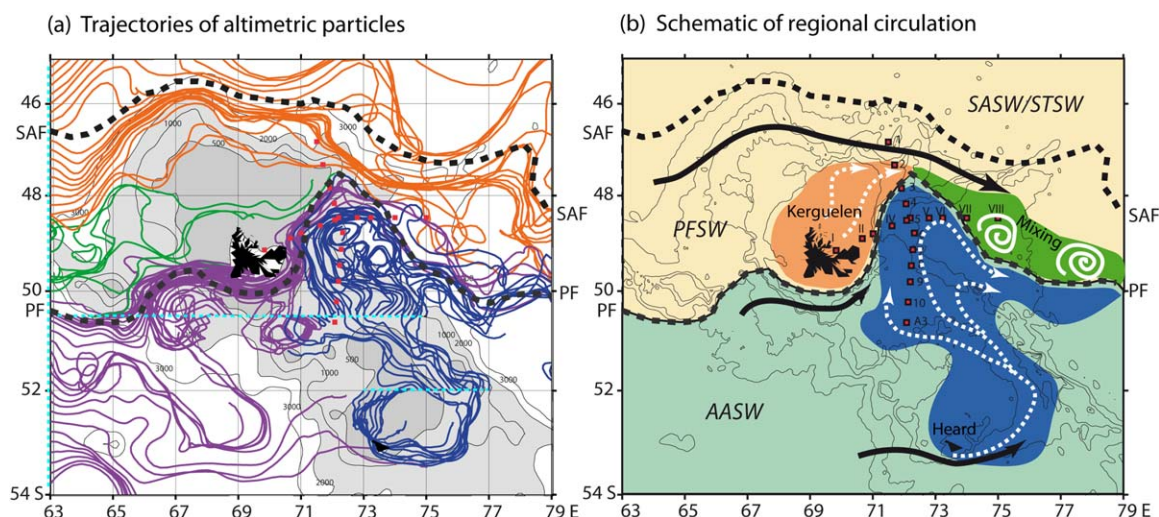
Figure 15. (a) Trajectories of artificial particles in the Kerguelen region forward tracked using the altimetric velocity time series fields. Initial positions of particles are indicated by cyan dashed lines. See the text for the details of the methodology. The SAF and PF are shown by thick black dashed lines. (b) A schematic of the circulation of surface/subsurface waters drawn based on Figure 15a. The abbreviations are Antarctic Surface Water (AASW), Polar Frontal Surface Water (PFSW), Subantarctic Surface Water (SASW), and Subtropical Surface Water (STSW).

around the Kerguelen Islands. Consistent with our previous work, the newly determined PF location rounds the Kerguelen Islands from the south, executing a permanent cyclonic meandering in the off-plateau area immediately east of the Kerguelen Islands. Due to the northward deflection of the PF along the eastern escarpment east of the Kerguelen Islands, the shallow plateau waters southeast of the islands advance as far north as the northeastern corner of the Kerguelen Plateau, possibly affecting the regional primary production that has an important climatic implication.

By way of discussion of our findings within the context of the general circulation in the Kerguelen region, we present in Figure 15 a map of trajectories of artificial water particles tracked using the altimetric velocity time series and a resultant schematic of circulation of surface/subsurface waters of different origins. The altimetric velocity time series used for this tracking are those of fine resolution (1 day resolution in time and 1/8° in space for the 6 months of period starting from 1 April 2011) specially prepared for the KEOPS2 cruise by the AVISO/CLS. We applied a forward tracking algorithm similar to that employed by *Filippi et al.* [2010], which uses a simple prediction-correction scheme. Artificial particles are seeded at every 0.1° (cyan dashed lines in Figure 15a) along 63°E between 45° and 54°S in the upstream area of the Kerguelen Plateau, along 50°30′S between 63° and 75°E south of the Kerguelen Islands, and along 52°S between 73° and 77°E north of the Heard Island. Different colors are used for emphasizing different pathways or sources of particles. It is remarkable that most trajectories forming the PF (purple lines) originate from the southwest of the Kerguelen Islands south of 50°S. However, the particles impinging on the Kerguelen Plateau from the west between 51° and 53°S do not show any well-organized zonal flow directly crossing over the plateau but they are hindered by topography, revealing a very irregular and stagnant eddying flow; only a few trajectories pass directly to the south of the Heard Island. The circulation around the latter island is clearly anticyclonic (blue lines) and extends northwestward over the eastern plateau to reach as far north as the northernmost reach of the PF at the northeastern corner of the Kerguelen Plateau.

The shallow shelf (<200 m) widely developed north of the Kerguelen Islands appears also as an effective barrier to the zonal circulation, and only 3 out of 10 particles seeded between 49° and 50°S at 63°E (green lines) arrive at the shelf northeast of the islands after 6 months of tracking, indicating a very sluggish zonal flow less than 5 cm s^{-1} in general. On the other hand, the particles seeded north of 48°30′S at 63°E (orange lines) round the shelf from the north, flowing along the northern escarpment of the Kerguelen Plateau. To the east of 68°E, they begin to bend gradually to the south to approach most closely the northernmost PF located near 72°E. In the area north of the PF downstream of 73°E, several trajectories originating from different latitudes intermingle, indicating the existence of strong mesoscale eddy activity, thus possibly promoting enhanced cross-frontal exchange or mixing of different water masses.

These altimetric particle trajectories are remarkably consistent with the frontal circulation discussed in the previous sections. A schematic of the regional circulation of surface/subsurface waters (Figure 15b) is intended for providing the reader with a larger scale perspective for better understanding the pathways or origins of different water masses flowing into the off-plateau study area east of the Kerguelen Islands. It is clear that most of the KEOPS2 stations except for a few stations at the transect extremities encounter the Antarctic Surface Water (AASW) originating from the shallow shelf surrounding the Heard Island. This southern shelf water is completely separated by the PF from the northern shelf water north of the Kerguelen Islands, which is embedded within the Polar Frontal Surface Water (PFSW) rounding the northern shelf along the northern escarpment of the Kerguelen Plateau. These surface/subsurface waters coming from different places meet and undergo eddy mixing along the southward retroflecting PF to the east 73°E.

Finally, we hope that the newly determined PF and its associated circulation shall serve as a reference for better interpreting other variables and biogeochemical parameters measured during the KEOPS2 cruise and for erasing definitely the long-standing confusion about the PF location in the Kerguelen region. In addition, considering an increasing volume of hydrographic data in the Southern Ocean especially thanks to Argo float measurements, reliable satellite altimetry, and the urgent need for a precise determination of the PF for climate-related studies, a similar investigation as the present work is warranted to extend to other critical ACC frontal zones, in particular in the vicinity of islands or prominent topographic features.

References

Belkin, I. M., and A. L. Gordon (1996), Southern Ocean fronts from the Greenwich Meridian to Tasmania, *J. Geophys. Res.*, *101*, 3675–3696.

Blain, S., et al. (2007), Effect of natural iron fertilization on carbon sequestration in the Southern Ocean, *Nature*, *446*, 1070–1074, doi:10.1038/nature05700.

Botnikov, V. N. (1963), Geographical position of the Antarctic convergence zone in the Pacific Ocean, *Sov. Antarct. Exped. Inf. Bull., Engl. Transl.*, *4*, 324–327.

Bown, J., M. Boye, P. Laan, A. R. Bowie, Y.-H. Park, C. Jeandel, and D. M. Nelson (2012), Imprint of a dissolved cobalt basaltic source on the Kerguelen Plateau, *Biogeosciences*, *9*, 5279–5290.

Bretherton, F., R. Davis, and C. Fandry (1976), A technique for objective analysis and design of oceanographic experiments applied to MODE-73, *Deep Sea Res. Oceanogr. Abstr.*, *23*, 559–582.

Filippi, J.-B., T. Komatsu, and K. Tanaka (2010), Simulation of drifting seaweeds in East China Sea, *Ecol. Informatics*, *5*, 67–72.

Gilles, S. T. (1994), Mean surface height of the Antarctic Circumpolar Current from Geosat data: Method and application, *J. Geophys. Res.*, *99*, 18,255–18,273.

Hummon, J. M., and E. Firing (2003), A direct comparison of two RDI shipboard ADCPs: A 75-kHz ocean surveyor and a 150-kHz narrow band, *J. Atmos. Oceanic Technol.*, *20*, 872–888.

McCartney, M. S., and K. A. Donohue (2007), A deep cyclonic gyre in the Australian-Antarctic basin, *Prog. Oceanogr.*, *75*, 675–750.

Moore, J. K., M. R. Abbott, and J. G. Richman (1999), Location and dynamics of the Antarctic Polar Front from satellite sea surface temperature data, *J. Geophys. Res.*, *104*, 3059–3073.

Nowlin, W. D., Jr., and J. M. Klinck (1986), The physics of the Antarctic Circumpolar Current, *Rev. Geophys. Space Phys.*, *24*, 469–491.

Orsi, A. H., T. Whitworth III, and W. D. Nowlin Jr. (1995), On the meridional extent and fronts of the Antarctic Circumpolar Current, *Deep Sea Res., Part I*, *42*, 641–673.

Park, Y.-H., and F. Vivier (2011), Circulation and hydrography over the Kerguelen Plateau, in *The Kerguelen Plateau: Marine Ecosystem and Fisheries*, edited by G. Duhamel et al., pp. 43–55, Cybium, Paris.

Park, Y.-H., L. Gambéroni, and E. Charriaud (1993), Frontal structure, water masses and circulation in the Crozet Basin, *J. Geophys. Res.*, *98*, 12,361–12,385.

Park, Y.-H., N. Gasco, and G. Duhamel (2008a), Slope currents around the Kerguelen Islands from demersal longline fishing records, *Geophys. Res. Lett.*, *35*, L09604, doi:10.1029/2008GL033660.

Park, Y.-H., J. L. Fuda, I. Durand, and A. C. Naveira Garabato (2008b), Internal tides and vertical mixing over the Kerguelen Plateau, *Deep Sea Res., Part II*, *55*, 582–593.

Park, Y.-H., F. Roquet, I. Durand, and J. L. Fuda (2008c), Large-scale circulation over and around the Northern Kerguelen Plateau, *Deep Sea Res., Part II*, *55*, 566–581.

Park, Y.-H., F. Vivier, F. Roquet, and E. Kestenare (2009), Direct observations of the ACC transport across the Kerguelen Plateau, *Geophys. Res. Lett.*, *36*, L18603, doi:10.1029/2009GL039617.

Roquet, F., Y.-H. Park, C. Guinet, F. Bailleul, and J.-B. Charrassin (2009), Observations of the Fawn Trough Current over the Kerguelen Plateau from instrumented elephant seals, *J. Mar. Syst.*, *78*(3), 377–393, doi:10.1016/j.jmarsys.2008.11.017.

Ruddick, B. R., and J. S. Turner (1979), The vertical length scale of double diffusive intrusions, *Deep Sea Res., Part A*, *26*, 903–913.

Sokolov, S., and S. R. Rintoul (2009), Circumpolar structure and distribution of the Antarctic Circumpolar current fronts: 1. Mean circumpolar paths, *J. Geophys. Res.*, *114*, C11019, doi:10.1029/2008JC005108.

Testut, L., F. Birol, and C. Delebecque (2012), Regional tidal modeling and evaluation of Jason-2 tidal geophysical correction, *Mar. Geod.*, *35*, 299–313.

van Beek, P., M. Bourquin, J. L. Reyss, M. Souhaut, M. A. Charette, and C. Jeandel (2008), Radium isotopes to investigate the water mass pathways on the Kerguelen Plateau (Southern Ocean), *Deep Sea Res., Part II*, *55*, 622–637.

Visbeck, M. (2002), Deep velocity profiling using Lowered Acoustic Doppler Current Profilers: Bottom track and inverse solutions, *J. Atmos. Oceanic Technol.*, *19*, 794–807.

Whitworth, T., III, and W. D. Nowlin Jr. (1987), Water masses and currents of the Southern Ocean at the Greenwich Meridian, *J. Geophys. Res.*, *92*, 6462–6476.